

Evaluating an Alternative Model for the Input Function in FDG-PET Studies¹

Hongbin Guo² Rosemary A Renaut² Kewei Chen³

Abstract

A new model for an input function for human [¹⁸F]-2-Deoxy-2-fluoro-D-glucose fluoro (FDG) positron emission tomography (PET) brain studies with bolus injection is presented in [1]. Here this model is compared with other analytic models. Experiments which use data from 18 healthy subjects are designed to contrast the input model as compared to other functional and population-derived expressions. The new model provides an effective means to recover the input function in FDG-PET studies as compared to other models.

Key words: Input Function Estimation, FDG-PET, Quantification

1 Introduction

This report is a supplement to the paper [1], in which a new input function model is studied and validated for FDG-PET studies. Rate constants generated by plasma samples are compared with those using this new model, [1]. The focus of this report is to compare the analytic expression of the input function in [1] to other analytic expressions, [2], [3], [4], by directly fitting plasma samples. It is shown that the new model can approximate the input function with fewer plasma samples as compared to other expressions.

Email addresses: hb_guo@asu.edu (Hongbin Guo), renaut@asu.edu (Rosemary A Renaut), Kewei.Chen@bannerhealth.com (Kewei Chen).

¹ Supported by the Arizona Center for Alzheimer's Disease Research, funded by the Arizona Department of Health Services, and by NIH grant EB 2553301

² Department of Mathematics and Statistics, Arizona State University

³ Banner Alzheimer Institute and Banner Good Samaritan Positron Emission Tomography Center

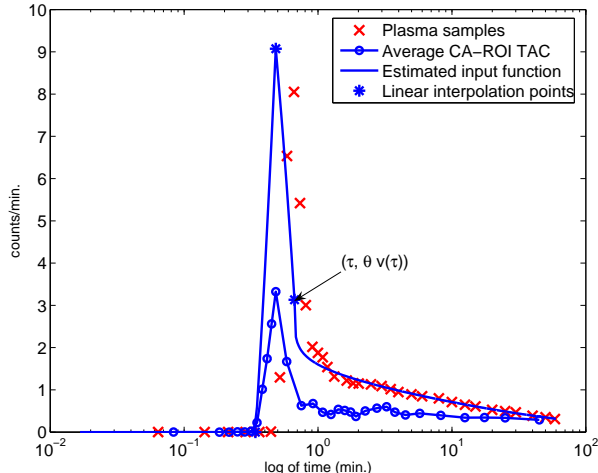


Fig. 1. Comparison of the arterial plasma samples (crosses), average CA-ROI region time activity curve (solid line with open circles) and estimated input function solid line with 3 discrete asterisks. Also illustrated, with the 3 asterisks, is the time at which the average tracer activity is initiated in the CA-ROI τ_0 , the time point for the peak value τ_p , the point of continuity τ between windows W_1 and W_2 , and the three plasma samples used for the fit. Time is expressed on logarithm scale hence emphasizing the effects for early time.

2 A Model for the Input Function

We distinguish between the characteristics of the input function over roughly the first half minute and later time. In the very early time after the tracer is rapidly administered, the input function as seen in the plasma, denoted by $u_p(t)$, increases rapidly to a peak value and then quickly drops, see crosses, Figure 1. This sharp increase and decrease can be approximated by two line segments, one upward from left of the peak to the peak, and one downward from the peak. Three nodes $(\tau_0, 0)$, (τ_p, v_p) and (τ, v_τ) , which define the line segments, are generated using image-derived data from carotid artery regions of interest (CA-ROIs). Here $v(t)$ denotes the average image-derived whole blood time activity curve of the CA-ROIs and the linear segments are scaled to account for partial volume effects and red cell fraction (hematocrit).

After the early interval of roughly one half minute, image-derived data are subject to greater contamination of tracer spillover from tissue to blood. We therefore model the input data after the initial interval without using image-derived data, but using a limited number of intravenous plasma samples. The piecewise-continuous parameter-dependent formulation for the estimated in-

put function u_e is given by

$$u_e(t, \theta, \lambda, \delta) = \begin{cases} 0 & t \in [0, \tau_0] \\ \theta v_p \frac{t - \tau_0}{\tau_p - \tau_0} & t \in [\tau_0, \tau_p] \\ \theta \frac{v_\tau (t - \tau_p) + v_p (\tau - t)}{\tau - \tau_p} & t \in [\tau_p, \tau] \\ \theta v_\tau e^{-\lambda(t - \tau)^\delta} & t > \tau. \end{cases} \quad (1)$$

Here the interval $[0, \tau]$ defines the early time window W_1 , typically $\tau < 0.6$ minutes and $W_2 = [\tau, T]$ is the second window, $T \approx 60$ minutes. The parameter θ is introduced to account for partial volume effects and hematocrit in the measurement of the tracer concentration in $v(t)$.

To estimate the model parameters θ , λ and δ , we use information from images and three plasma samples. Input data for early time, roughly up to 0.6 minutes, are obtained non-invasively from the time activity curve measured from a carotid artery region of interest (CA-ROI). Representative tissue time activity curves are obtained by clustering the output curves to a limited number of dominant clusters, [5]. Three venous plasma samples at later time are used to fit the functional form of the input function in conjunction with obtaining kinetic rate parameters of the dominant clusters, K_1 , k_2 and k_3 using the compartmental model for FDG-PET, for details see [1] or Appendix. In this report, we compare $u_D = Ae^{-\lambda(t - \tau)^\delta}$ with other functional expressions by fitting the plasma samples.

3 Alternative models

We consider four alternative representations of the input function for $t \geq \tau$:

$$u_A = A_1 e^{-\lambda_1(t - \tau)} + A_2 e^{-\lambda_2(t - \tau)} + A_3 e^{-\lambda_3(t - \tau)}, \quad (2)$$

$$u_B = (A_1(t - \tau_0) - A_2 - A_3) e^{-\lambda_1(t - \tau_0)} + A_2 e^{-\lambda_2(t - \tau_0)} + A_3 e^{-\lambda_3(t - \tau_0)}, \quad (3)$$

$$u_C = A e^{-\lambda(t - \tau)}, \quad (4)$$

$$u_D = A e^{-\lambda(t - \tau)^\delta}. \quad (5)$$

u_A is widely used, [2], while u_B is the modification of u_A as suggested in [3,4]. Both are dependent on 6 parameters A_i , λ_i , $i = 1, 2, 3$, and are designed to model the input data for the entire time window. The third form u_C assumes simple exponential decay after time τ and the fourth is its modification used in defining u_e , dependent on just three parameters A , λ , and δ .

Table 1

The mean and standard deviation of the root mean square error over all subjects for fitting u_p by functions (2)- (5), and for different choices for τ . All plasma samples with $t \geq \tau$ are used in the data fit.

j	u_A	u_B	u_C	u_D
1	.049 ± .022	.042 ± .019	.158 ± .061	.047 ± .025
2	.0331 ± .016	.029 ± .016	.086 ± .038	.038 ± .018
3	.027 ± .012	.023 ± .012	.067 ± .026	.034 ± .017
4	.020 ± .009	.015 ± .008	.059 ± .025	.024 ± .012

4 Contrasting fit to plasma samples of different input models

To investigate the suitability of (1) for fitting plasma-sampled data as compared to the standard models, retrospective PET data collected for a previous study were used, [6]. That study was designed to assess the use of the CA-ROI combined with limited plasma sampling for estimating the input data, whereas here the data is used to assess the efficacy of the alternative functional form of the input for improving estimates of the kinetic parameters. The arterial plasma samples were drawn every 5 seconds for the first minute, every 10 seconds for the second minute, every 30 seconds for the next 2 minutes, and then at 5, 6, 8, 10, 12, 15, 20, 25, 30, 40, 50 and 60 minutes, yielding a discrete representation of the plasma sampled function with units counts/ml/minute, denoted by $u_p(t_j)$, for $j = 1, \dots, 34$.

In Table 1 we report mean and standard deviation of the root mean square error over all 18 subjects for data fitting to plasma samples $u_p(t)$, $t \geq \tau$, for selected choices for τ , and all equations (2-5). The selection for τ is $\tau = t_{k+j}$, $j = 1, \dots, 4$, where t_k is the time at which the peak is achieved, $t_k = \tau_p$. The data used are all plasma samples $u_p(t)$ where $t \geq \tau$. The results confirm previous studies, [2-4]. Both u_A and u_B provide much better fits than u_C . They also slightly outperform the fit using u_D , but using six rather than just three parameters.

The routine implementation of the proposed method in [1] does not use all the plasma samples, but requires just three venous plasma samples taken at approximately $t = 10, 30$ and 60 minutes. Therefore, we assess u_D to model the input for $t \geq \tau$ but using a nonlinear least squares fit based on just three plasma samples taken on the interval from roughly 10 to 60 minutes along with given data at time τ , but with the error in the model calculated over all time points $t > \tau$, see Table 2.

This test highlights that u_D provides a good fit over the entire interval using a limited number of data points, as is also illustrated for a representative case (subject 5) in Figure 2. The order of magnitude of the error is relatively

Table 2

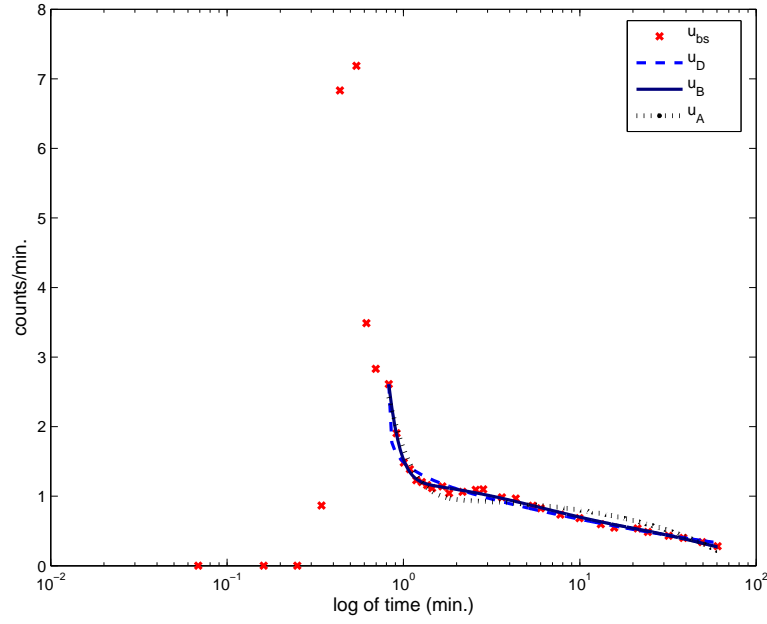
The mean and standard deviation of the root mean square error over all subjects for fitting u_p by functions (2)- (5), and for different choices for τ . All plasma samples with $t \geq \tau$ are used in calculating the error but for the data fit only the points at $t = \tau$ and $t > 10$ minutes are used.

j	u_A	u_B	u_C	u_D
1	3.39 ± 1.1	$.49 \pm .5$	$.60 \pm .3$	$.06 \pm .03$
2	$.11 \pm .08$	$.13 \pm .1$	$.20 \pm .1$	$.048 \pm .02$
3	$.11 \pm .06$	$.10 \pm .1$	$.12 \pm .06$	$.044 \pm .02$
4	$.12 \pm .1$	$.045 \pm .02$	$.12 \pm .06$	$.029 \pm .01$

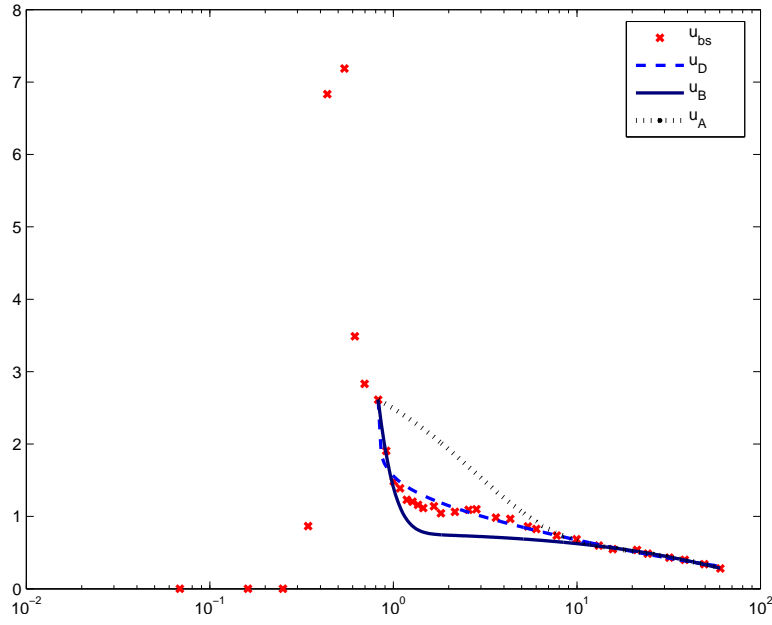
insensitive to the choice of τ and, as would be expected, is smaller for larger τ , for which the interval of the data fit is smaller, and over which the variation in u_p is much less.

5 Conclusion

In summary, u_D which depends on only three unknown parameters is able to find the best fit to u_p if the goal is to use a limited number of later time plasma samples.



(a) Fitting with $t > \tau$



(b) Fitting with $t > 10$ minutes and $t = \tau$

Fig. 2. Here (a) illustrates how a good fit to u_p is obtained with u_A , u_B and u_D using all plasma samples with $t > \tau$. In comparison, (b) shows how u_A and u_B fail to accurately capture u_p when the fitting does not use points between τ and 10 minutes. Illustrated in each case is the fit for representative subject 5, where τ is the third plasma sample after the peak.

Appendix – Algorithm for recovering the input function

In the compartmental model [7] for FDG-PET, the ideal TTAC $y(t)$ at a given voxel, or for a specific brain tissue ROI, is given analytically by convolution (\otimes) of the instantaneous response function (IRF) with input $u(t)$

$$y(t) = u(t) \otimes \left(\frac{K_1 k_3}{k_2 + k_3} + \frac{K_1 k_2}{k_2 + k_3} e^{-(k_2 + k_3)t} \right). \quad (6)$$

The IRF is the term within the parentheses and depends on the specific tissue response to the tracer. K_1 is the transport rate from plasma to brain tissue with units ml/100g/minute, k_2 is the transport rate back from brain to blood vessel with units 1/minute, k_3 is the phosphorylation rate of intra-cellular FDG by hexokinase enzymes to FDG-6-phosphate with units 1/minute. Because the scanning interval 60 minutes is relatively small, it will be difficult to accurately estimate the dephosphorylation rate of intra-cellular FDG-6-phosphate back to FDG, k_4 , [8]. We thus set k_4 , which is itself small, to zero.

Typically, kinetic parameters for cluster curve $y^{(i)}$, given by (6), can be obtained by the minimization of $\Phi^{(i)}$,

$$\Phi^{(i)}(\mathbf{x}^{(i)}, \alpha^{(i)}) = \sum_{j=1}^n w_j \left(y_{\text{TAC}}^{(i)}(t_j) - \alpha^{(i)} \cdot y^{(i)}(t_j) - (1 - \alpha^{(i)}) \cdot u(t_j) \right)^2. \quad (7)$$

$\alpha^{(i)}$ accounts for both partial volume and spillover effects for cluster i , and the rate constants are components of $\mathbf{x}^{(i)} = [K_1^{(i)}, k_2^{(i)}, k_3^{(i)}]$. The contributions from each time point are weighted by w_j . Ideally, these are the inverse of the variances of the data of each frame and are different for different tissue TACs. Because of the difficulty of estimating the variances they are set to the time durations of the relevant time frames as practiced in [9]. To define a feasible space for the parameters bound constraints are imposed.

It is usually assumed that the values for $u(t_j)$ used in (7) are measured values of the input function. In contrast, we intend the use of the functional form (1). With respect to the dominant first cluster, the parameters θ , λ , δ of the input function $u_e(t)$ can be recovered simultaneously with the kinetic rate constants. This is accomplished in a two-stage process. Specifically, notice that for any given value of θ , parameters λ , δ can be obtained as the solutions of

$$[\lambda(\theta), \delta(\theta)] = \operatorname{argmin}_{\lambda, \delta} \sum_{l=1}^3 \left[\theta v(\tau) e^{-\lambda(\tilde{t}_l - \tau)^\delta} - u_p(\tilde{t}_l) \right]^2, \quad (8)$$

using three intravenous plasma samples, $(\tilde{t}_l, u_p(\tilde{t}_l))$, $l = 1, 2, 3$. Therefore, at each iteration in the minimization of $\Phi^{(1)}(\mathbf{x}^{(1)}, \alpha^{(1)}, \theta)$, noting now the introduced dependence on the recovery coefficient θ , (8) can be solved to obtain

the updates of λ and δ .

To make the estimation of the input function more robust, we note that the input function is common to all TTACs and thus propose that the optimization be performed simultaneously over p clusters with cost function

$$\Phi(\mathbf{x}, \alpha, \theta) = \sum_{i=1}^p \Phi^{(i)}(\mathbf{x}^{(i)}, \alpha^{(i)}, \theta) \quad (9)$$

where $\mathbf{x} = (\mathbf{x}^{(1)}, \dots, \mathbf{x}^{(p)})$, and $\alpha = (\alpha^{(1)}, \dots, \alpha^{(p)})$.

In summary, the nested optimization method, illustrated in the flow chart provided in Figure 3, is formulated as follows

$$\min_{\mathbf{x}, \alpha, \theta} \Phi(\mathbf{x}, \alpha, \theta) \quad \text{subject to constraints} \quad (10)$$

$$\begin{aligned} 1.2 \leq \theta \leq 4, \quad 0.9 \leq \alpha^{(i)} \leq 1, \\ 0.015 \leq K_1^{(i)} \leq 0.3, \quad 0.024 \leq k_2^{(i)} \leq 0.54, \quad 0.01 \leq k_3^{(i)} \leq 0.2. \end{aligned} \quad (11)$$

Matlab 7.0 function `fmincon` from the optimization toolbox version 3.0.2 [10] is utilized for carrying out this constrained minimization. The bounds used are based on experimental results [8] for both gray and white matter from 13 subjects, but with doubling of upper bounds and halving of lower bounds such that the feasible space is not too conservatively estimated. Time delay between the TTACs and the input function is removed by automatically shifting the TTACs such that the first peak of each is aligned with v_{τ_p} .

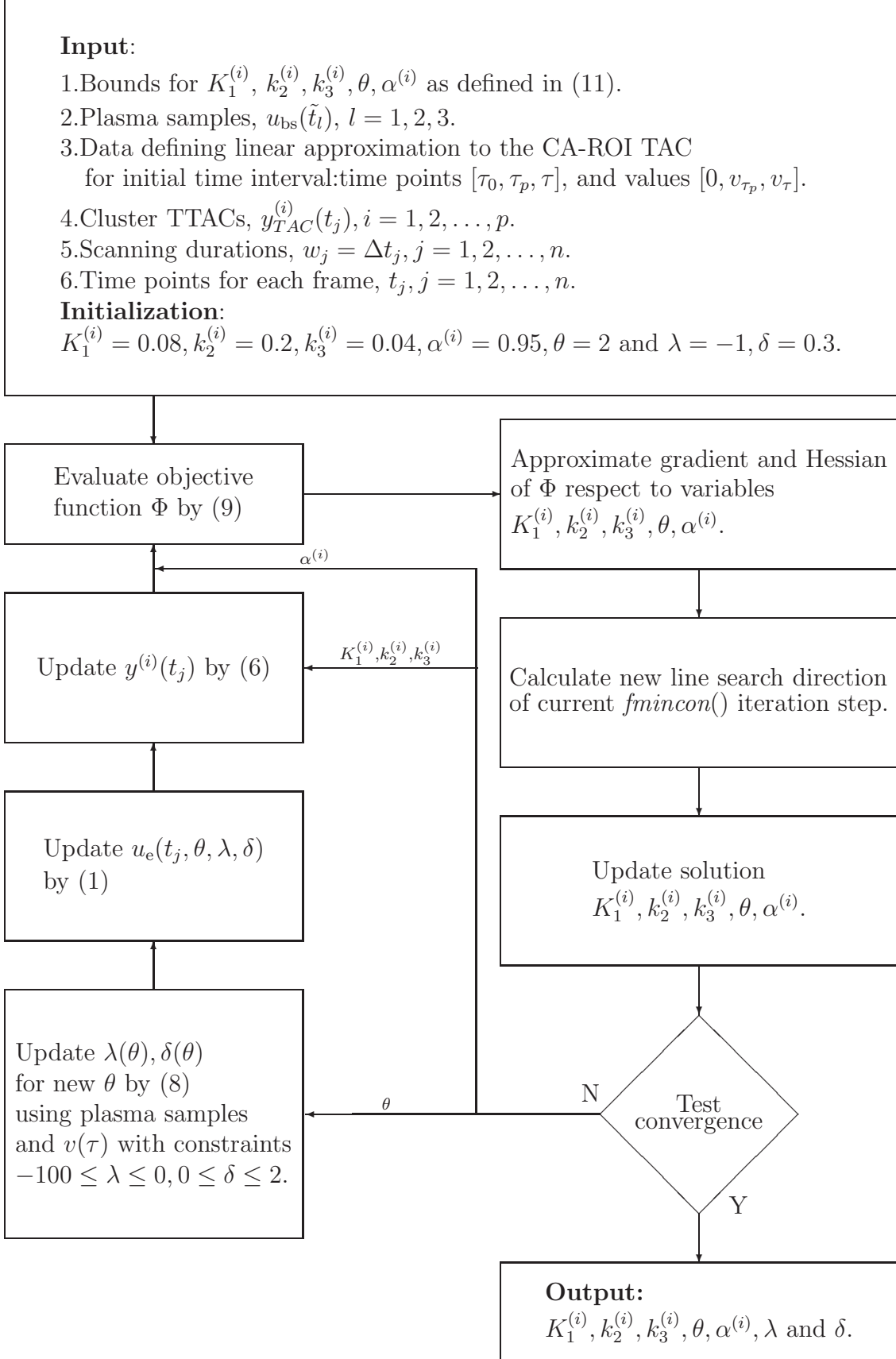


Fig. 3. Flow chart detailing the steps of the nested optimization.

References

- [1] H. Guo, R. Renaut, K. Chen, Improved imaged-derived input function for study of human brain FDG-PET, 2007, submitted.
- [2] M. E. Phelps, S.-C. Huang, E. J. Hoffman, C. E. Selin, D. Kuhl, Tomographic measurement of local cerebral glucose metabolic rate in man with (^{18}F) fluorodeoxyglucose: Validation of method, *Ann. Neurol.* 6 (1979) 371–388.
- [3] D. Feng, S.-C. Huang, X. Wang, Models for computer simulation studies of input functions for tracer kinetic modeling with positron emission tomography, *Int. J. Biomed. Comput.* 32 (1993) 95–110.
- [4] K.-P. Wong, D. Feng, S. R. Meikle, M. J. Fulham, Simultaneous estimation of physiological parameters and the input function - In vivo PET data, *IEEE J. ITBM* 5 (1) (2001) 67–76.
- [5] H. Guo, R. A. Renaut, K. Chen, E. Reiman, Clustering huge data sets for parametric PET imaging, *Biosystems* 71 (1-2) (2003) 81–92.
- [6] K. Chen, D. Bandy, E. Reiman, S.-C. Huang, M. Lawson, D. Feng, et al, Noninvasive quantification of the cerebral metabolic rate for glucose using positron emission tomography, ^{18}F -fluorodeoxyglucose, the Patlak method, and an image-derived input function, *J. Cereb. Blood Flow Metab.* 18 (1998) 716–723.
- [7] L. Sokoloff, M. Reivich, C. Kennedy, M. H. D. Rosiers, C. S. Patlack, K. D. Pettigrew, et al, The [^{14}C] deoxyglucose method for the measurement of local cerebral glucose metabolism: theory procedures and normal values in the conscious and anesthetized albino rat, *J. Neurochem.* 28 (1977) 897–916.
- [8] S.-C. Huang, M. E. Phelps, E. J. Hoffman, K. Sideris, C. J. Selin, D. E. Kuhl, Noninvasive determination of local cerebral metabolic rate of glucose in man, *Am. J. Physiol.* 238 (E) (1980) 69–82.
- [9] Y. Zhou, C. J. Endres, J. R. Brasic, S.-C. Huang, D. F. Wong, Linear regression with spatial constraint to generate parametric images of ligand-receptor dynamic PET studies with a simplified reference tissue model, *NeuroImage* 18 (4) (2003) 975–989.
- [10] The Mathworks, Optimization Toolbox User’s Guide, 2005.